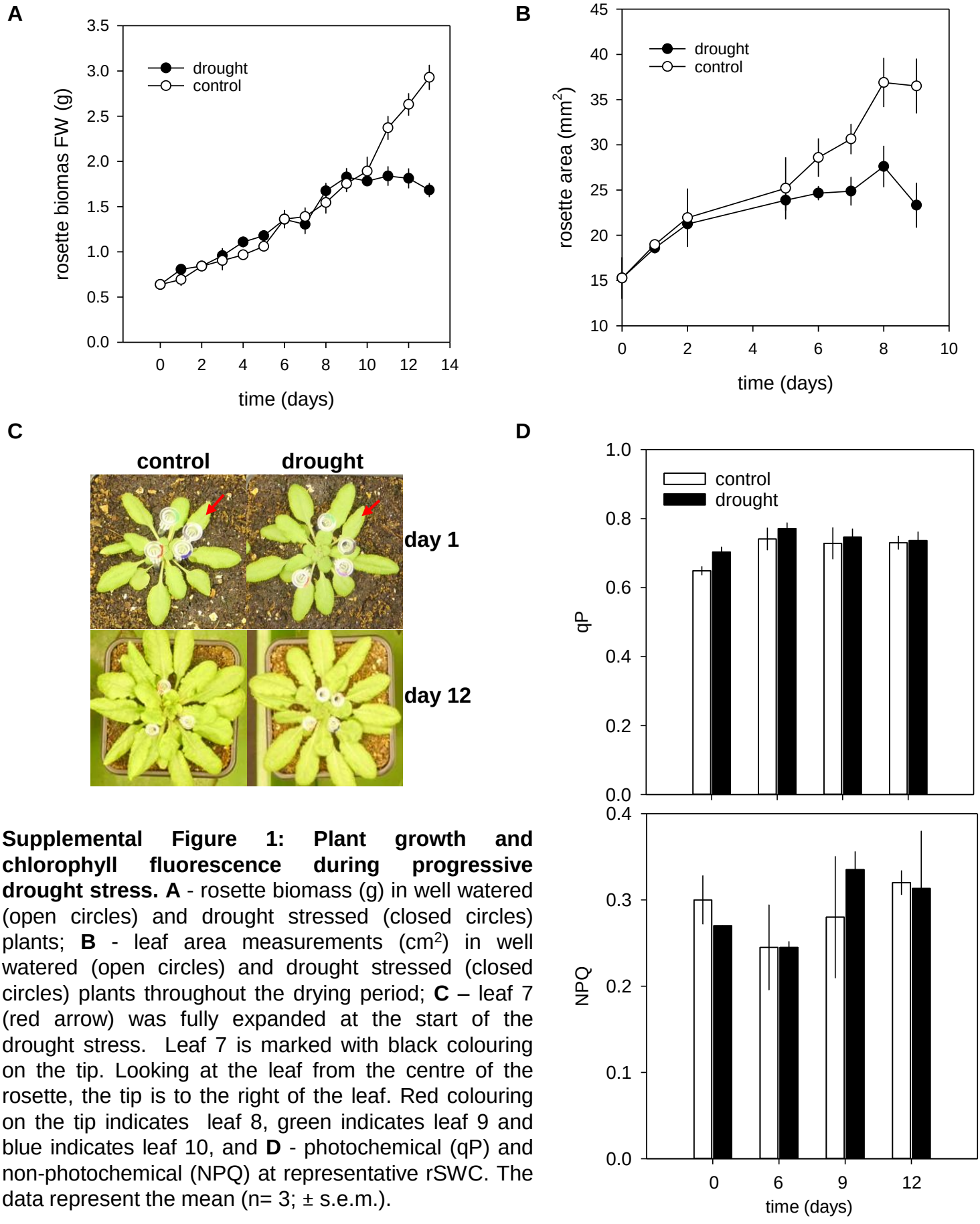

Supplemental Figure 1: Plant growth and chlorophyll fluorescence during progressive drought stress. A - rosette biomass (g) in well watered (open circles) and drought stressed (closed circles) plants; **B** - leaf area measurements (cm^2) in well watered (open circles) and drought stressed (closed circles) plants throughout the drying period; **C** – leaf 7 (red arrow) was fully expanded at the start of the drought stress. Leaf 7 is marked with black colouring on the tip. Looking at the leaf from the centre of the rosette, the tip is to the right of the leaf. Red colouring on the tip indicates leaf 8, green indicates leaf 9 and blue indicates leaf 10, and **D** - photochemical (qP) and non-photochemical (NPQ) at representative rSWC. The data represent the mean (n= 3; ± s.e.m.).

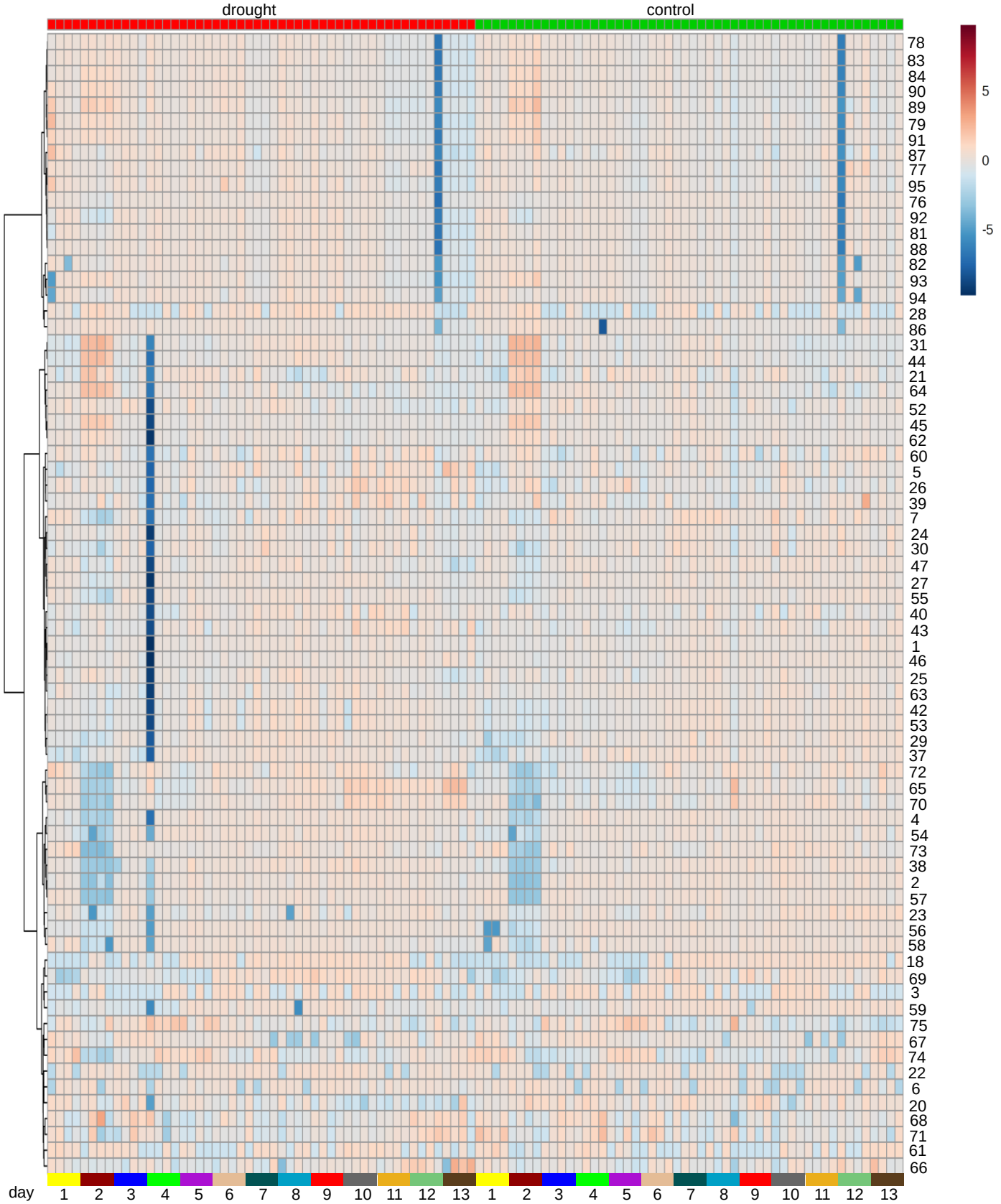

Supplemental Figure 2. Targeted metabolite analyses of secondary metabolites (except flavonoids), sugars and amino acids. Peak areas were log2 transformed and mean-centered and divided by standard deviation. The metabolites are clustered (Pearson distance and Ward clustering). Analysis was carried out with MetaboAnalyst 2 (Xia et al., 2012). Raw data and ANOVA are shown in Supplemental Data Set 1 (see key for compounds), Supplemental Data Set 2 (see key for compounds) and Supplemental Data Set 3.

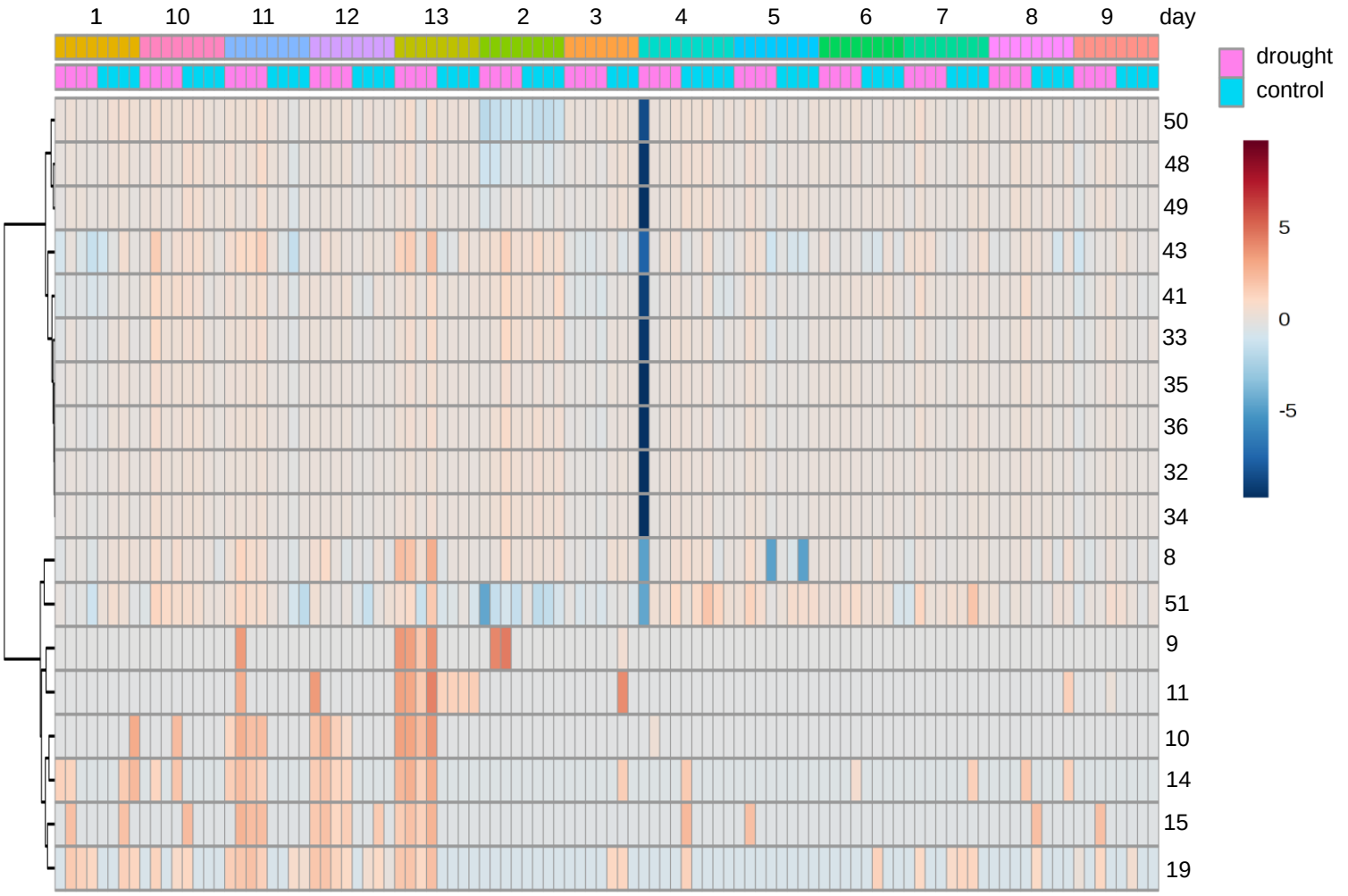

Supplemental Figure 3: Targeted metabolite analyses of flavonoids and anthocyanines. Peak areas were log2 transformed and mean-centered and divided by standard deviation. Analysis was carried out as described in Supplemental Figure 2. Raw data and ANOVA are shown in Supplemental Data Set 1 (see key for compounds), Supplemental Data Set 2 (see key for compounds) and Supplemental Data Set 3.

A

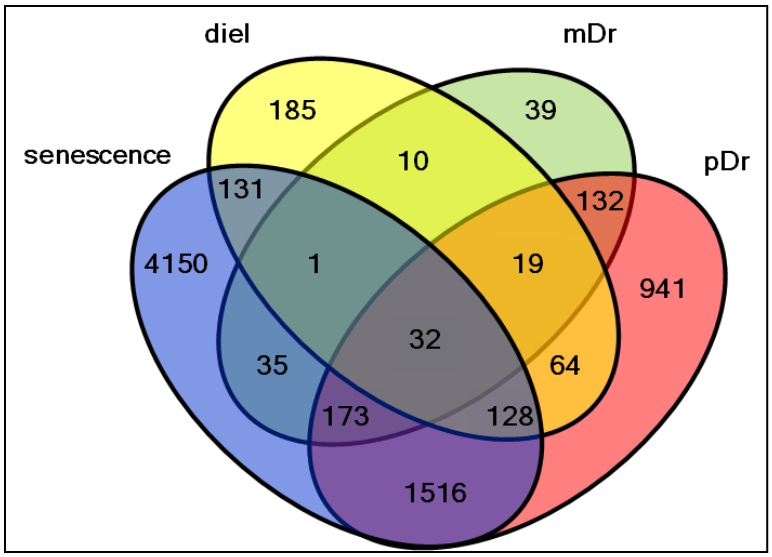

B

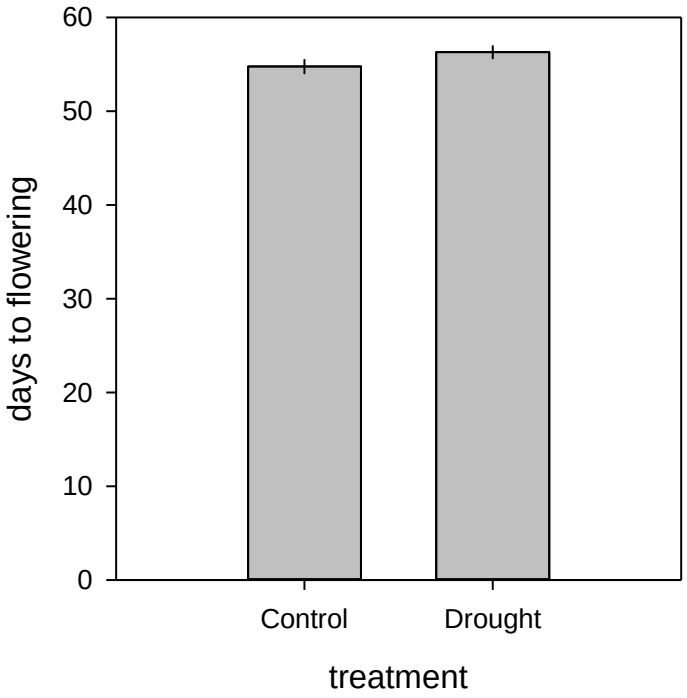

Supplemental Figure 4: The impact of drought stress on plant development. A – Comparative meta-analysis of the publicly available drought datasets (Harb et al., 2010; Wilkins et al., 2010) with a publicly available leaf 7 senescence time-series dataset (Breeze et al., 2011); mDr – moderate drought, pDr – progressive drought, diel – diurnal drought, and senescence – time series senescence**.** The Venn diagram shows the overlap of the 3 drought treatments - and senescence DEGs, and **B** - Flowering time in well watered and drought stressed Arabidopsis wild type plants. Col-0 plant were grown under short day conditions as described in the Methods section. At 5 weeks plants were subjected to progressive drought stress. When 17% rSWC was reached, plants were re-watered and flowering time was recorded as days after sowing. Control plants were maintained well watered (n=15, ± ser)

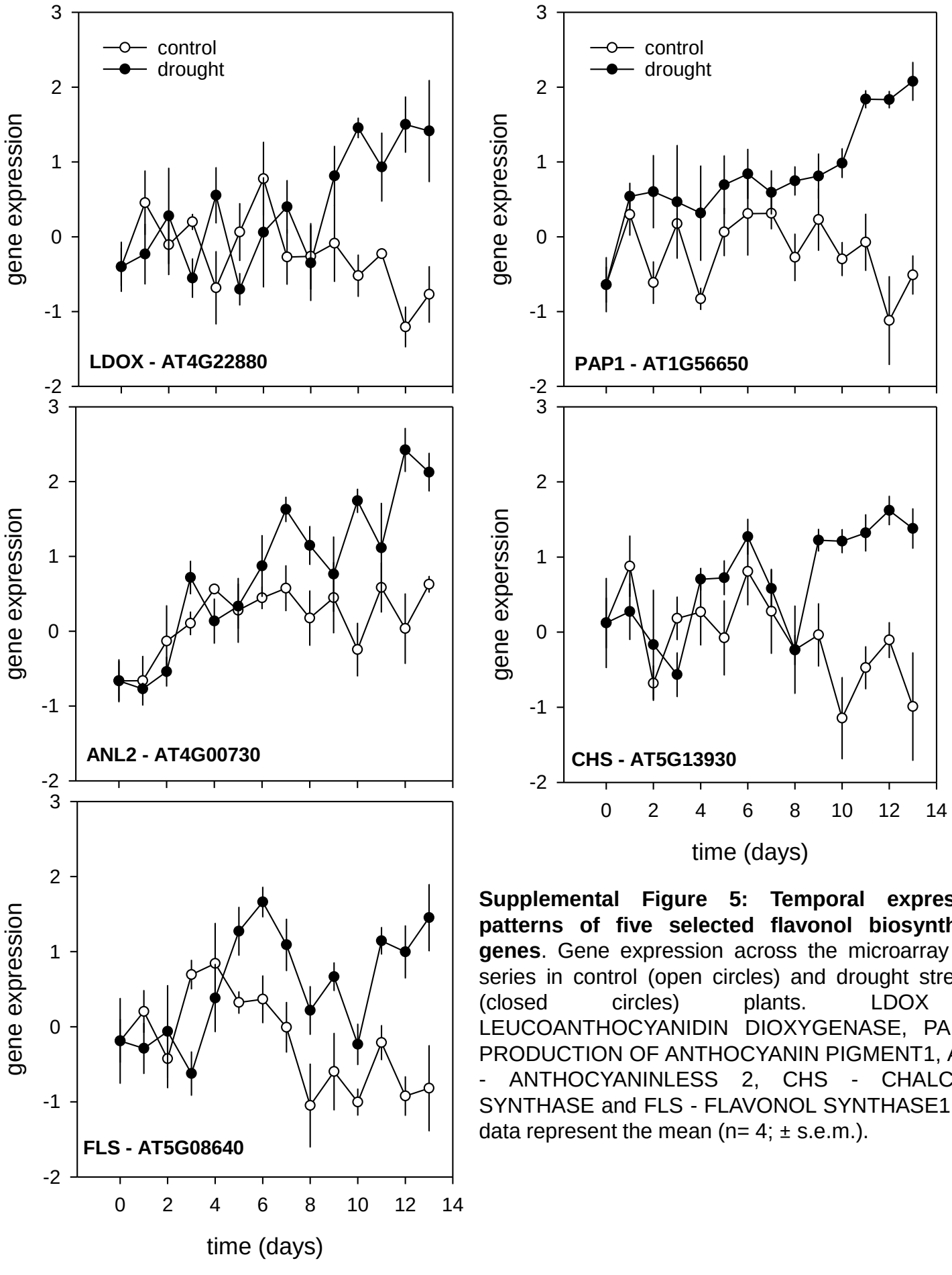

Supplemental Figure 5: Temporal expression patterns of five selected flavonol biosynthesis genes. Gene expression across the microarray time series in control (open circles) and drought stressed (closed circles) plants. LDOX - LEUCOANTHOCYANIDIN DIOXYGENASE, PAP1 - PRODUCTION OF ANTHOCYANIN PIGMENT1, ANL2 - ANTHOCYANINLESS 2, CHS - CHALCONE SYNTHASE and FLS - FLAVONOL SYNTHASE1. The data represent the mean (n= 4; ± s.e.m.).

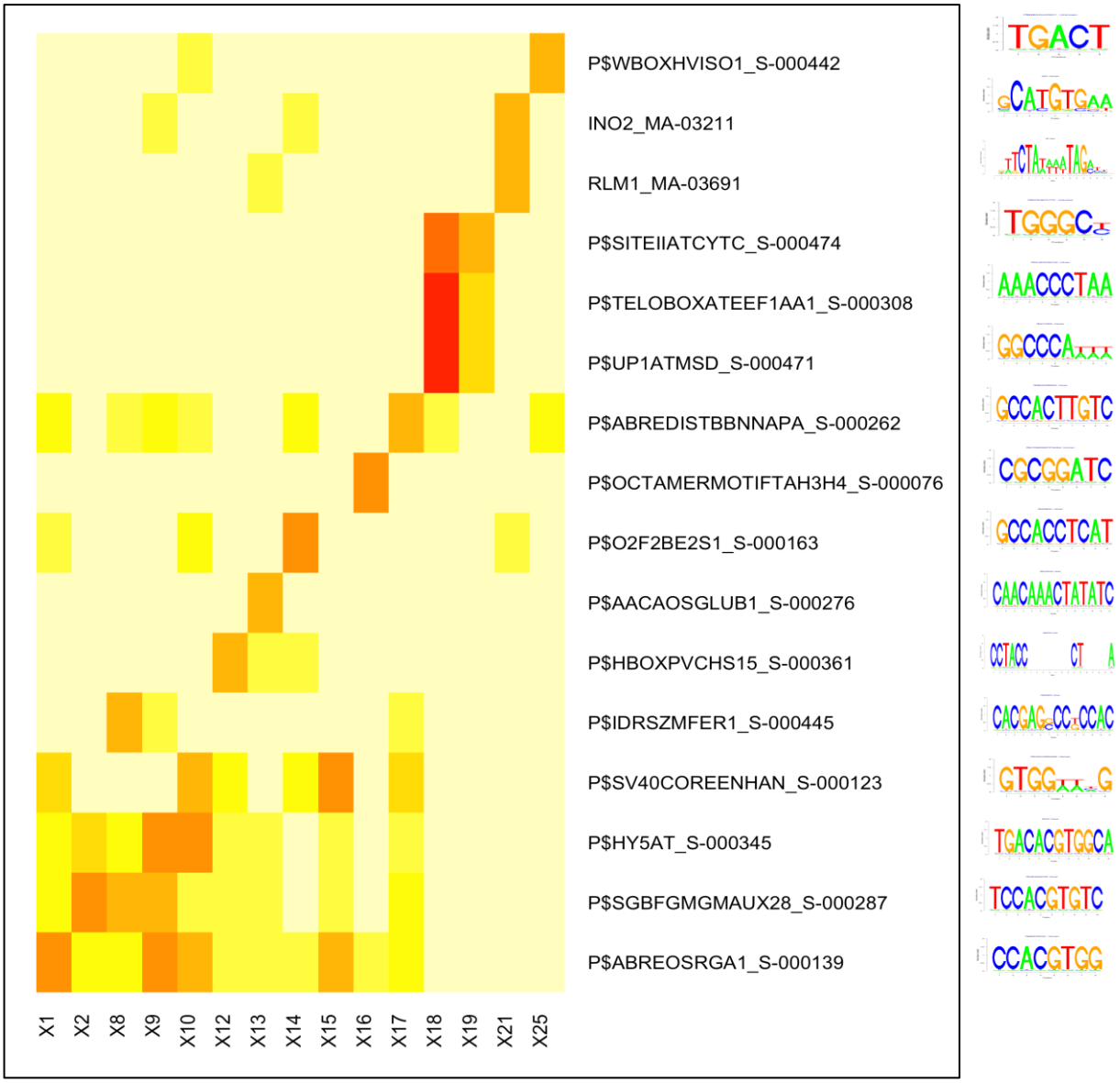

Supplemental Figure 6: **Analysis of TF binding sites**. Over-representation of known TF binding motifs in promoters of gene clusters. Cluster names are given on the horizontal axis, names and sequence logo representations of known TF binding motifs (where character size indicates nucleotide frequency) are shown on the vertical axis. Coloured boxes correspond to raw P values, and only rows/columns where at least one cluster-motif pairing shows significant enrichment are shown (full results available in Supplemental Data Set 13).

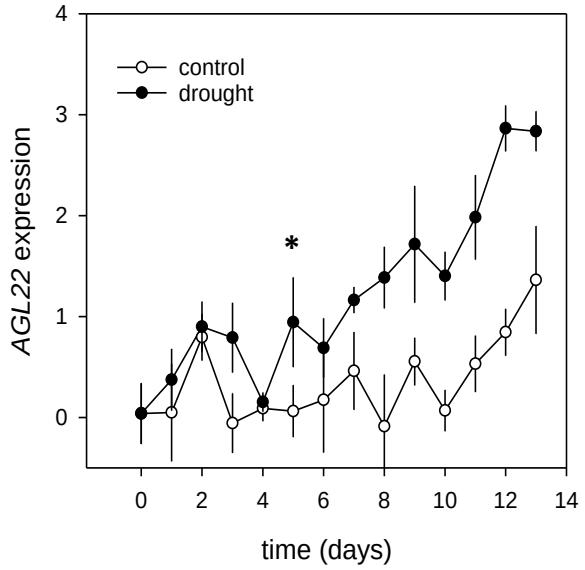

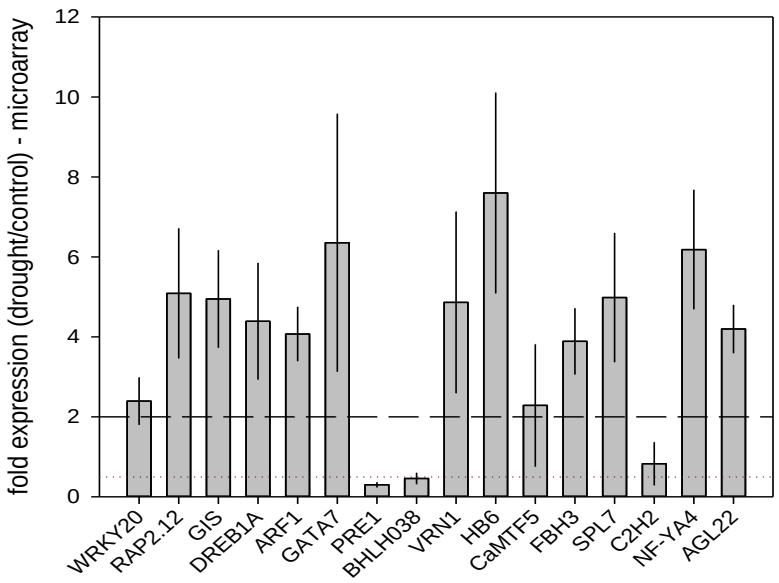

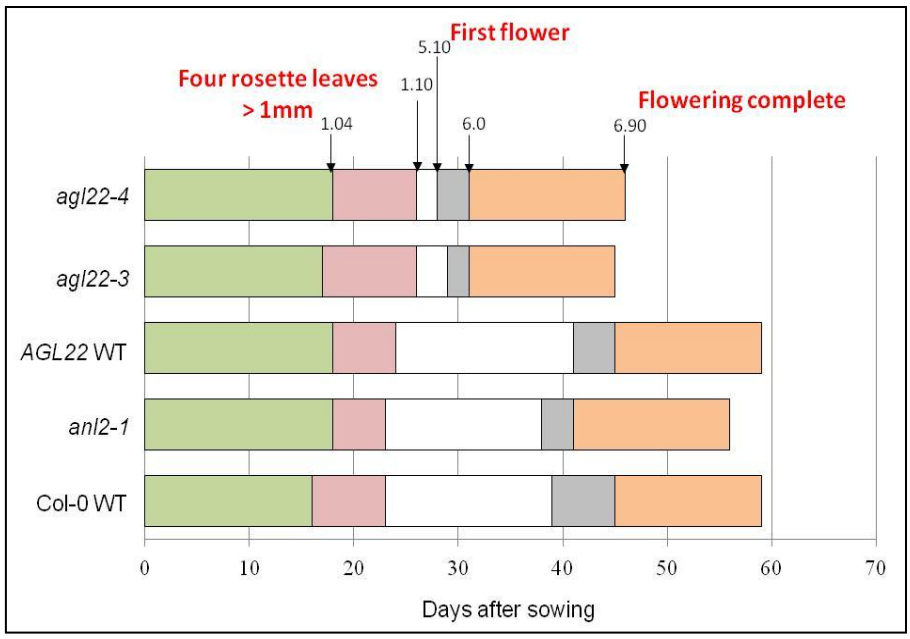

Supplemental Figure 7: Gene expression of selected drought responsive genes and growth analysis of *agl22* mutants. A - *AGL22* expression across the time series in control (open circles) and drought stressed (closed circles) plants, indicating an early rise in *AGL22* during drought. The star represents the time of first differential expression (Supplemental Data Set 4); **B** - fold expression of selected differentially expressed TF genes calculated at day 12 of the microarray time-series experiments (for abbreviations see Supplemental Data Set 14), and **C** - growth analysis according to Boyes et al., 2001 for *agl22*-3 and *agl22*-4, compared to Col-0, segregating WT (*AGL22-WT*) and non-developmental mutant (*anl2*-1). The blue line indicates the time at which drought stress was performed.

A

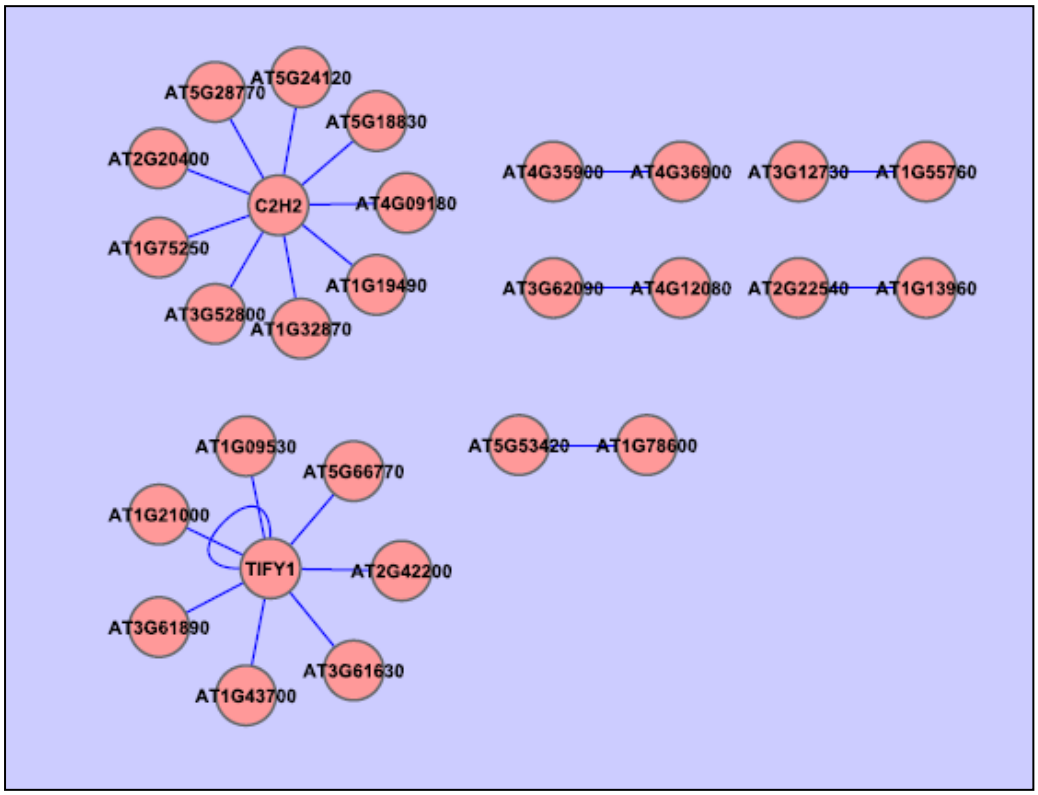

B

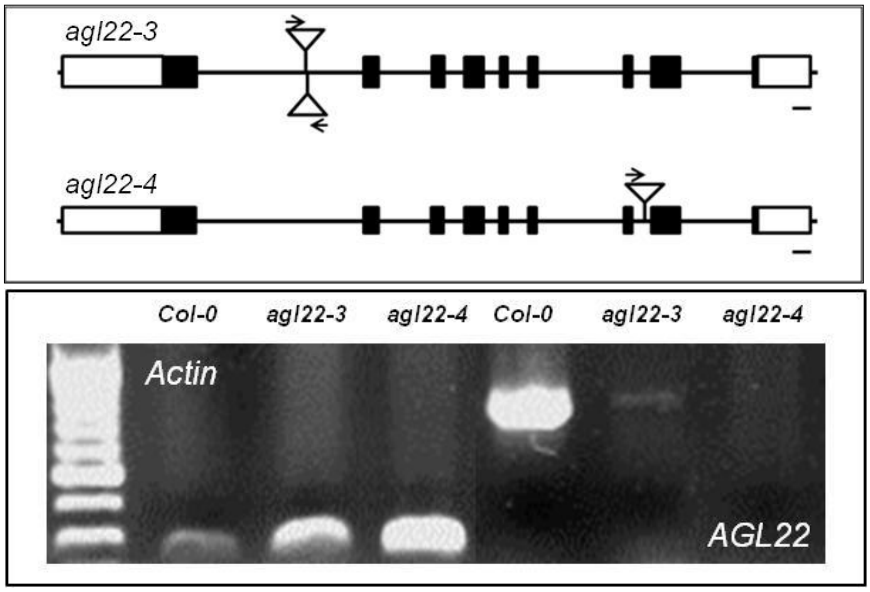

Supplemental Figure 8: Validation of the knockout phenotype in *agl22* insertion mutants and the specific role of *AGL22* during drought stress. A - gene regulatory networks generated using the control time series data (threshold z-score = 1.65). No significant network emerged from the network modelling of the control dataset, and **B** - location of T-DNA insertions in *agl22-3* and *agl22-4* and RT-PCR of the full length *AGL22* transcript.

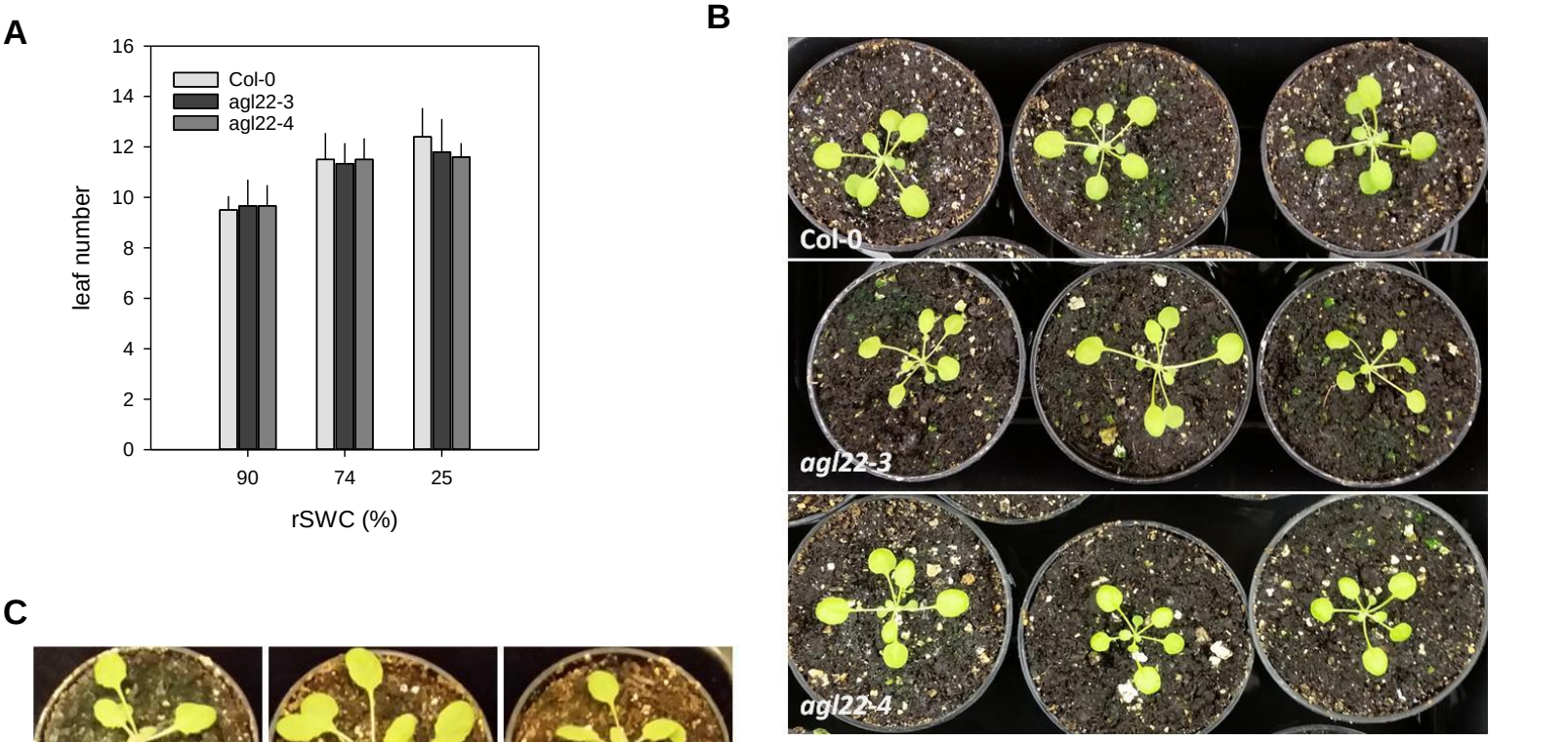

Supplemental Figure 9: Growth and photosynthetic phenotype of *agl22* mutants during drought stress A – rosette leave number of Col-0, *agl22-3* and *agl22-4* mutants plants at different soil water contents (n=6); **B** – Col-0, *agl22-3* and agl22-4 mutants at day 22 prior to the start of the drought experiment, **C** - Col-0, *agl22-3* and *agl22-4* mutants at day 31 after 9 days of water withdrawal and **D** – light response curves in Col-0, *agl22-3* and *agl22-4* at different rSWC (n=5).

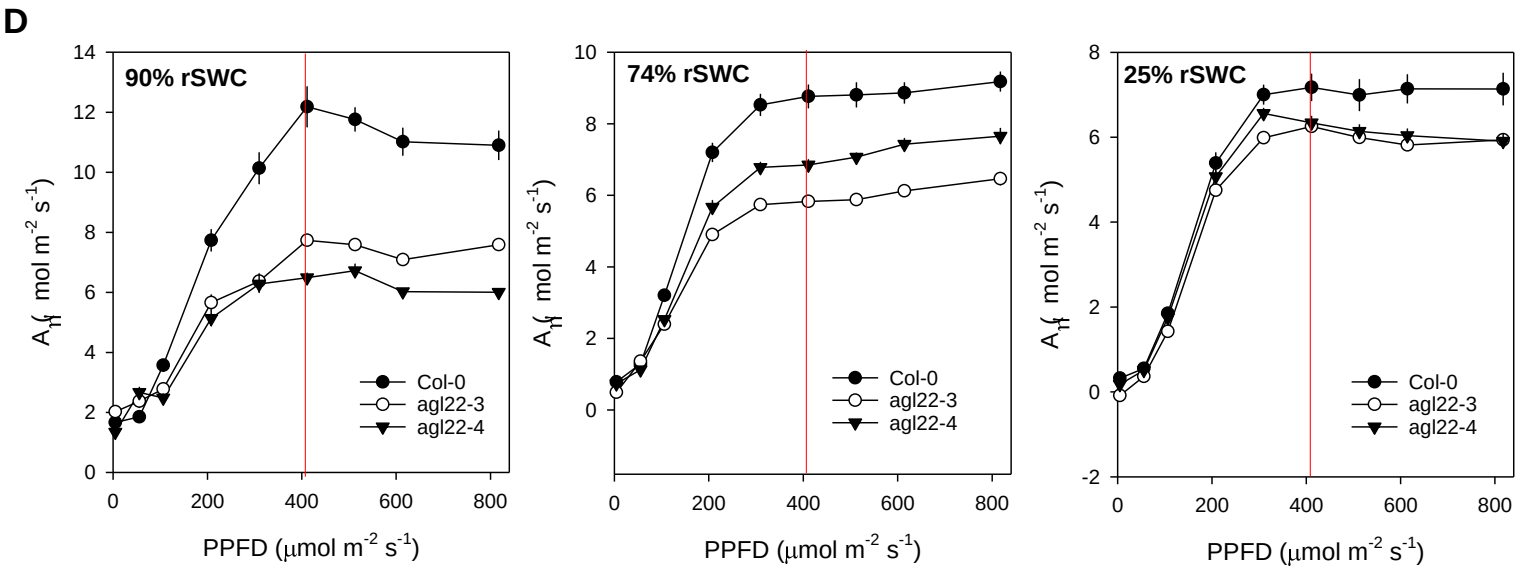

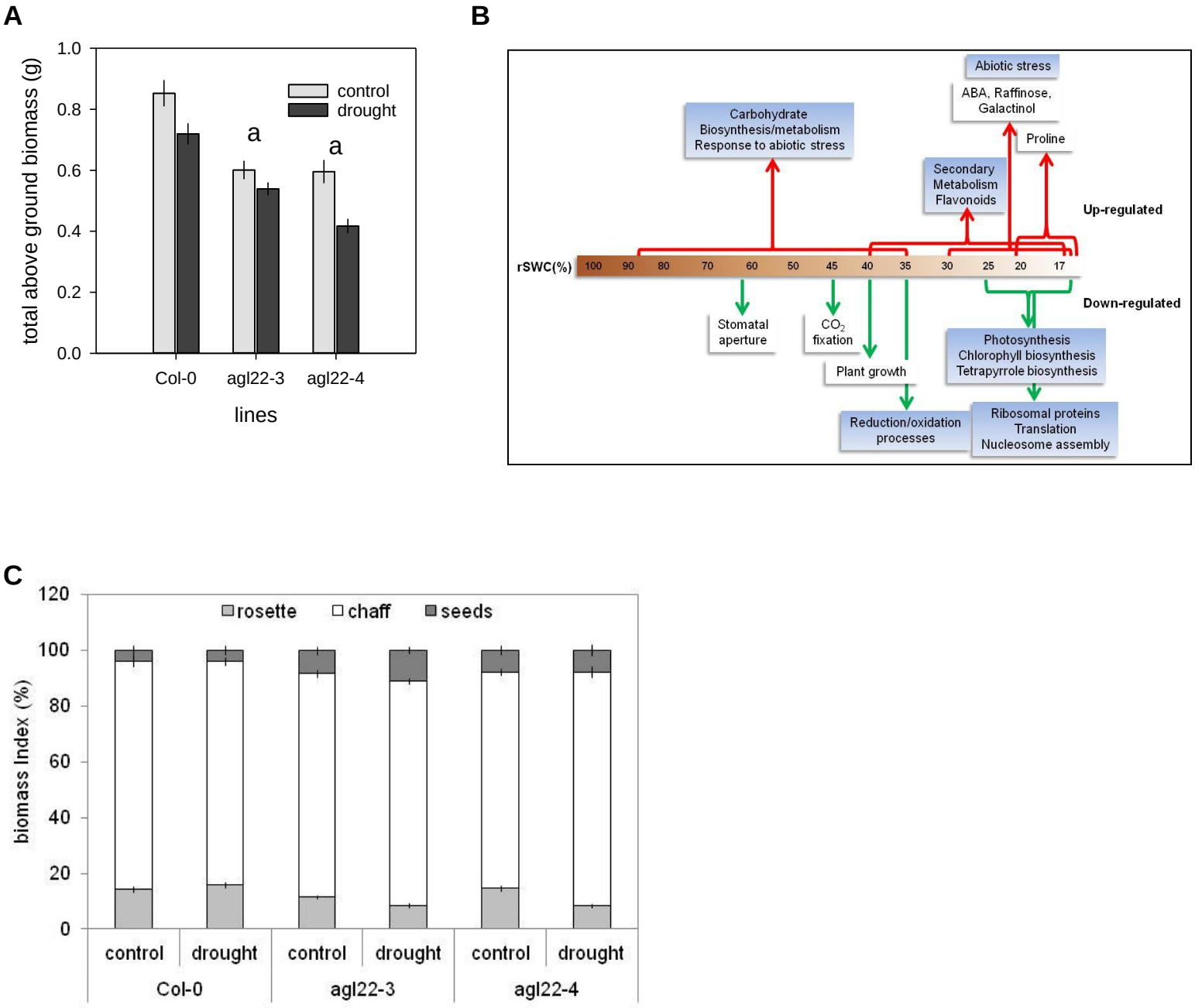

Supplemental Figure 10: Biomass production in *agl22* mutants compared to wild-type and timeline of events. A – total above ground biomass of *agl22-3* and *agl22-4* (n = 8). The data represent the mean (± s.e.m.). The letter a indicates significant difference between mutants and Col-0 at $p < 0.05$; **B** - biological and metabolic processes enriched across the drought transcriptome time-series (blue boxes). Changes in metabolites, plant growth and physiology are indicated in the white boxes. Enriched GO terms were identified using DAVID (Huang et al., 2008), and **C** – above ground biomass distribution (biomass index; %) under control and drought stress conditions.

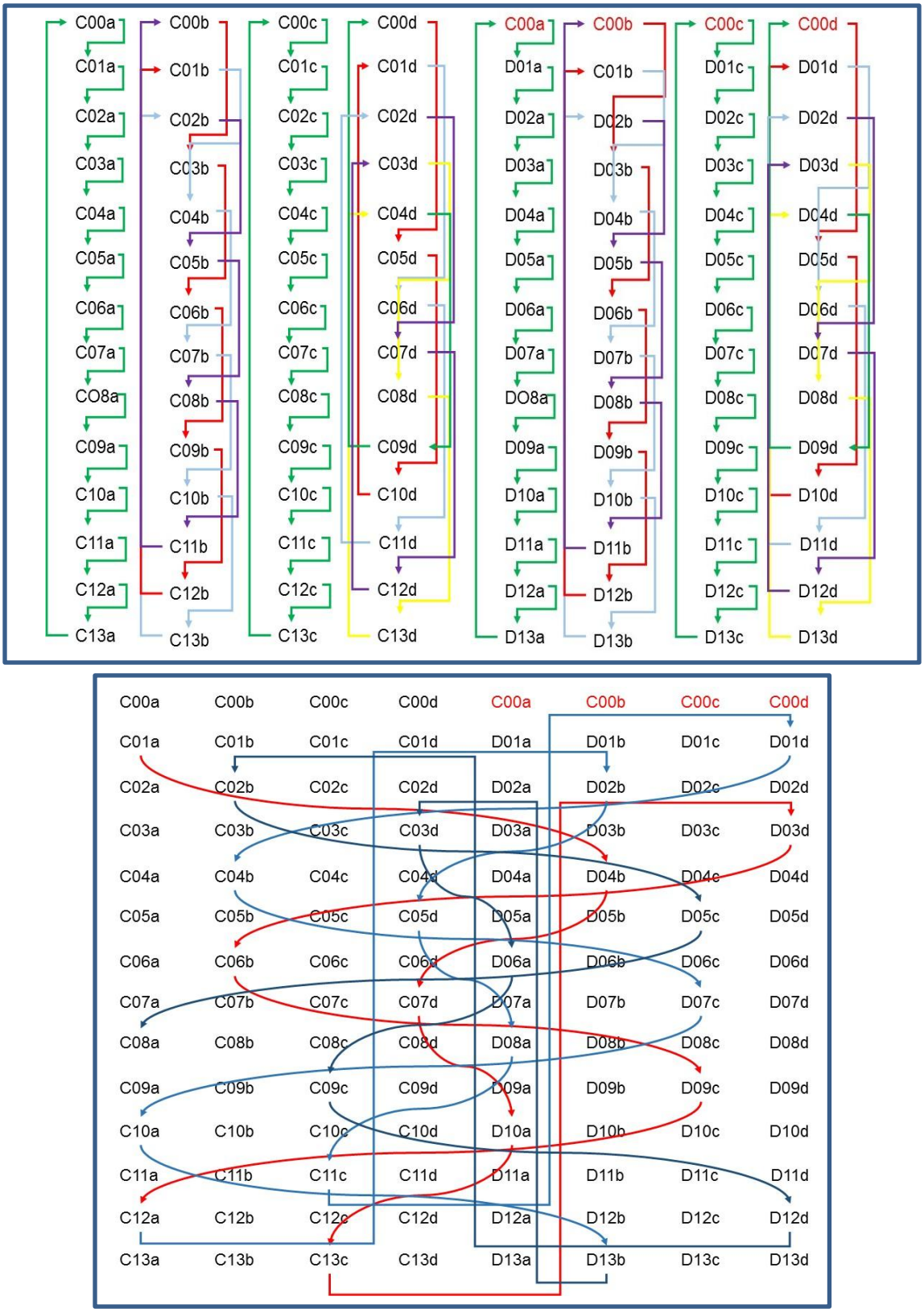

Supplemental Figure 11: **Schematic overview of array hybridisations across the 13 time points and two different treatments.** CO indicates well-watered control sample, and D indicates the drought stressed samples. The numbers from zero to thirteen indicate the days of the experiment. Small letters a – d indicate biological replicates. Lines between samples represent hybridisations across the time-series and treatments.

A

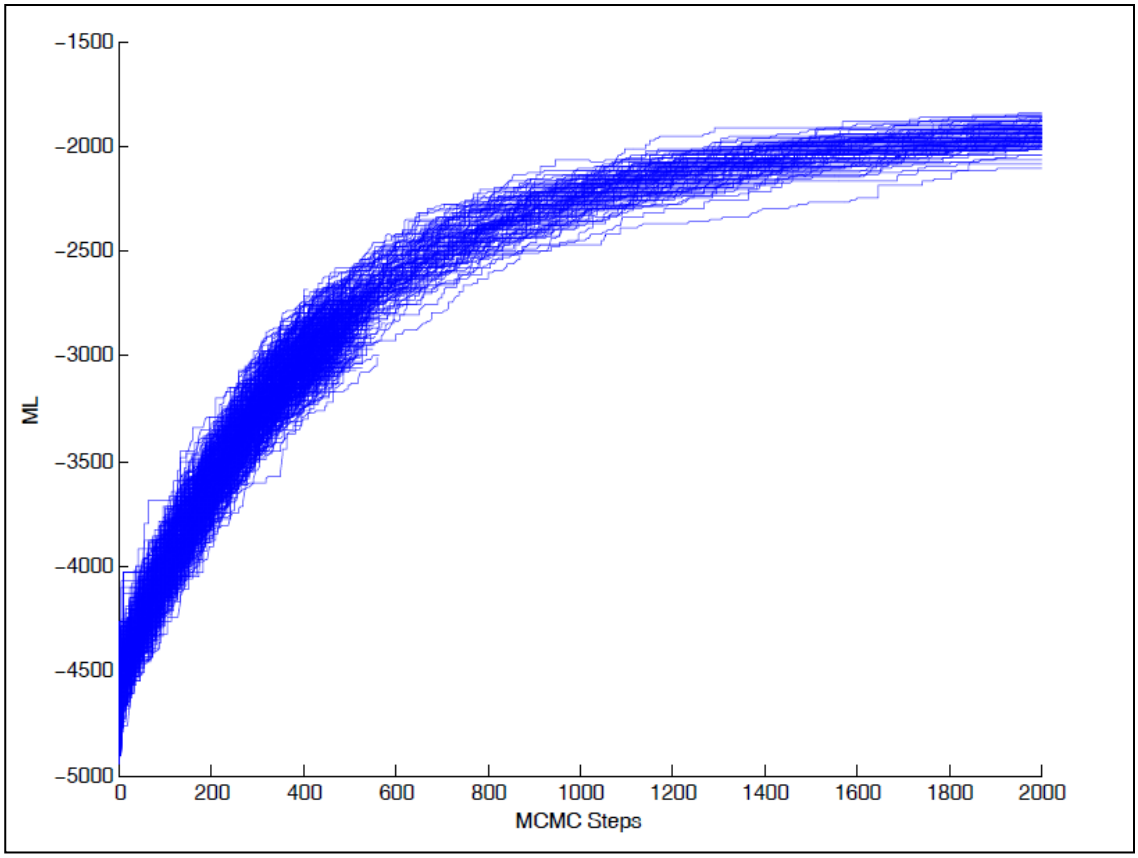

B

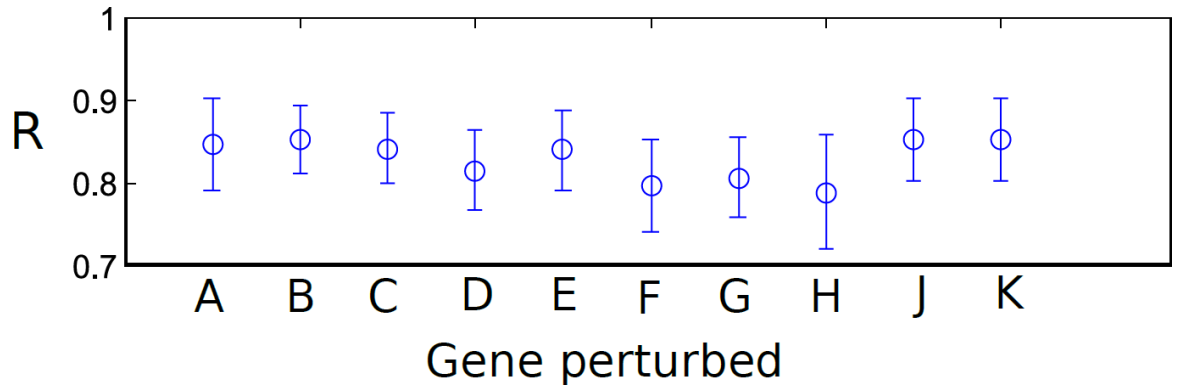

Supplemental Figure 12: **Validation of the M-VBSSM approach. A** – Example plateauing of the Marginal Likelihood around step 2000. Here different traces represent the likelihoods built around different genes, **B** - M-VBSSM was used to identify sets of genes to model together data from the network outlined in Zak et al. (2003). In general the M-VBSSM approach was able to correctly identify most to the genes to model (see Supplemental Methods).

.

Supplemental Table 1: primers for qPCR, mutant screen and RT-PCR analyses

Primer Name	Sequence	Locus ID
DREB1A F	TGAGATGTGTGATGCGACGAC	AT4G25480
DREB1A R	AAACATCGCCTCATCGTGCA	AT4G25480
WRKY20 F	CTGGCCGAGATGAGAAGGGA	AT4G26640
WRKY20 R	CGCTTCTCCACCATCGTCAG	AT4G26640
GIS F	CGTCGAATCCTTCTCTCAGC	AT3G58070
GIS R	AGAGAAATCTCTGCCGGTGA	AT3G58070
AGL22 F (qPCR)	CTCTCCGTTCTCTGCGACG	AT2G22540
AGL22 R (qPCR)	GGGCGTGATCACTGTTCTCA	AT2G22540
AGL22 F (RT-PCR)	ATGGCGAGAGAAAAGATTC	AT2G22540
AGL22 R (RT-PCR)	CTAACCACCATACGGTAAGC	AT2G22540
Actin 2A	AAGCTGGGGTTTTATGAATGG	AT3G18780
Actin 2B	GACTACGTGAACACACACTGTT	AT3G18780
Cyclophilin F	TCTTCCTCTTCGGAGCCATA	AT2G29960
Cuclophilin R	AAGCTGGGAATGATTCGATG	AT2G29960
GATA7 F	TGGAGAATGGGTCCATTAGG	AT4G36240
GATA7 R	TGGTGAATGTTGGGCTACAA	AT4G36240
HB6 F	TTGTGAAAATGGAGCAGACG	AT2G22430
HB6 R	TGATCAACGGTGGAGTACCA	AT2G22430
RAP2.12 F	TCGCCGATGTGAAACCATTC	AT1G53910
RAP2.12 R	ATTTCTCAGCGTCCCCATCC	AT1G53910
VRN1 F	TCCTTCTGGGTTTGCTGAGA	AT3G18990
VRN1 R	AGACATCGAACAGGCCATTG	AT3G18990
PRE1 F	TTGCCGGAGATTGGTCAACG	AT5G39860
PRE1 R	ACGCTCGCTCAGATTGTCAA	AT5G39860
BHLH038 F	AAAGGCGGTCCGCGAGTTAT	AT3G56970
BHLH038 R	TGGACGATGAGACTTGGAC	AT3G56970
ARF1 F	GGCAGACACTCCTTCCTCAG	AT1G59750
ARF1 R	GCCAAAAGGCTGATCCAATA	AT1G59750
CaMTF5 F	GCAAACGGCTGGAAACATTA	AT4G16150
CaMTF5 R	CCTTCAGGCTTTGCTCCTCT	AT4G16150
C2H2 F	GAGCAACCTTCCGTTTTCAA	AT4G17810
C2H2 R	ATCGAGCCAATGCTCTCATC	AT4G17810
FBH3 F	CCAGGGAGGGAGTTGTGCAT	AT1G51140
FBH3 R	CCCTTTTCACCACCACCACC	AT1G51140
SPL7 F	TTTTACCCGAAGCATCAACG	AT5G18830
SPL7 R	TCGCCATTAGAAGGTGAACG	AT5G18830
NFY-A4 F	TCAGGACGAAGTTCGGAATC	AT2G34720
NFY-A4 R	TGGAAGATACGCTTGCTGTG	AT2G34720
SAIL_LB1	GCCTTTTCAGAAATGGATAAATAGCCTTGCTTCC	
SALK_LBa1	TGGTTCACGTAGTGGGCCATCG	

Supplemental Methods

As the Metropolis Variation Bayesian State Space Modelling (M-VBSSM) has not been published previously, we outline the model selection approach that was used in the main text to identify potential hub genes involved in the drought response in more detail.

Model Comparison via a Metropolis Search

Let G represent a set of genes of interest (such as the set of all differentially expressed genes), some finite subset of which constitutes a core set, $\hat{S} \subset G$ which contains a particular gene of interest, i. Together this set forms a gene regulatory network. A key objective lies in identifying this set, as well as inferring the underlying network. Here we assume that the gene expression for any subset of genes is well modelled by a State Space model using the following coupled set of equations:

$$\boldsymbol{x}_t \propto A\boldsymbol{x}_{t-1} + B\boldsymbol{y}_{t-1} + \boldsymbol{w}_t,$$
$$\boldsymbol{y}_t = C\boldsymbol{x}_t + D\boldsymbol{y}_{t-1} + \boldsymbol{v}_t,$$

where $\boldsymbol{x}_t$ represents the hidden states at time t, $\boldsymbol{y}_t$ the vector of gene expression for the genes at time t, $\boldsymbol{w}_t$ and $\boldsymbol{v}_t$ represent additive Gaussian noise and A, B, C and D capture the topology and dynamics of the underlying gene regulatory network. Following Beal et al. (2005) we may estimate a distribution over these parameters using a variational approach. Within the Bayesian setting, a key indicator of the model fit for a particular set of genes, S_1 over a competing set of genes S_2 lies in comparing their marginal likelihoods $L(S_1)$ and $L(S_2)$ (see e.g. Vyshemirsky and Girolami, 2008). In theory, model comparison can be used to exhaustively compare all possible sets of genes of particular cardinality with that of model S_1 in order to identify sets of genes whose profiles have the highest probability of having been generated under the corresponding state space model. A distribution over these models might then be evaluated from their marginal likelihoods using Bayes' rule:

$$P(S_k|D) = \frac{P(D|S_k)P(S_k)}{\sum_j P(D|S_j)P(S_j)},$$

where, in order to ensure models are comparable, the summation in the denominator

has taken place over all combinations of genes of identical cardinality. Since $|G|$ is typically large, exhaustive enumeration is prohibitive and a Metropolis algorithm is instead used to search for a local set with sufficiently large marginal likelihood. A Metropolis approach may be used to search for models with high marginal likelihoods as follows:

1. First let J represent an initial set of genes with corresponding likelihood L(J) and complementary set $J^{'} = G \backslash J$.
2. A new set of genes, J_{new} , may generated by randomly swapping out N genes in $J \backslash i$ with an identical number of genes from J'.
3. The number of genes to be swapped is assumed to be Binomially distributed:

$$N \sim Binomial(\min(|J^{'}|, |J-1|), p),$$

where p is a random variable that may be tuned to ensure acceptance rates are optimal, and the maximum number of genes that can be swapped is $\min(|J^{'}|, |J-1|)$. The genes to be swapped are then chosen at random from their corresponding sets, and therefore represent a sample from a hypergeometric distribution. The new set of genes J_{new} may be then be accepted or rejected according the Metropolis rule:

$$P(accept) = \left(1, \frac{L(J_{new})p(J|J_{new})}{L(J)p(J_{new}|J)}\right),$$

where the forward and backward transition probabilities are given as products of Binomial and hypergeometric distributions which therefore cancel out. In this manner we may select genes that, when modelled alongside gene i using a Bayesian state space model, yield comparatively high marginal likelihoods. This approach may be used to systematically identify groups of genes to model with each gene from the larger list. After running the algorithm for sufficiently long periods of time, the marginal likelihood will plateau, as shown in Supplemental Figure 12A. Since we are only using this approach to achieve a preliminary ranking of genes, we opt to terminate the algorithm once the marginal likelihood plateaus, which occurs around step 2000. The networks at step 2000 are then used to compile summary network statistics, such as the number of times a given gene appears in a model, or the number of downstream connections it has.

Results

A preliminary test of the above algorithm was run on the *in silico* network of Zak et al. (2003), an ODE model describing 10 genes interacting via a total of 55 intermediates. This network incorporates many important biological network structures, including cascades, switches and auto-activation, complex kinetic interactions, including dimerisation/undimerisation and promoter binding/unbinding. For this reason, the Zak network is often employed as gold standard for the initial benchmarking of methods (Beal et. al., 2005; Penfold and Wild, 2011).

Using the Zak network, a series of WT time series profiles were simulated (indexed by $M = \{1, \ldots, 10\}$). Subsequently a perturbation set of profiles ($N = \{11, \ldots, 20\}$) were generated by perturbing the ligand injection, Q, and the two sets combined to give $G = M \cup N$.

In the MVBSSM the main goal is to identify as subset of genes that fit well together i.e., produce a model with a high marginal likelihood. We therefore chose to systematically build models around genes 1 through 10 i.e., the conditional set X was chosen to be systematically genes 1 through 10. The MVBSSM algorithm was run for 9000 iterations, allowing an additional 1000 steps for burn-in to identify 9 other genes to model alongside X. For each set J the following ratio could be calculated:

$$R = \frac{|J \cap M|}{|J|},$$

indicating the ratio of the number of genes in J that belong to the WT set M to the number of genes in J. Since the conditional set X belongs in M this ratio should high i.e., relatively few genes from N should belong with J. The results are summarised in Supplemental Figure 12B and show that the algorithm correctly identified the correct genes to model around a particular gene of interest. These scores suggest that the approach represents a useful way of identifying subsets of genes that warrant further, more specific network modelling.

Supplemental References

Beal, M. J., Falciani, F., Ghahramani, Z., Rangel, C., and Wild, D. L. (2005). A Bayesian approach to reconstructing genetic regulatory networks with hidden factors. *Bioinformatics* **21**: 349-356.

Penfold, C. and Buchanan-Wollaston, V. (2014). Modelling transcriptional networks in leaf senescence. *J Exp Bot* **65**: 3859-3873.

Vyshemirsky, V. and Girolami, M. A. (2008). Bayesian ranking of biochemical system models. *Bioinformatics* **24**: 833-839.

Windram, O., Penfold, C., and Denby, K. (2014). Network modeling to understand plant immunity. *Ann Rev Phytopath* **52**: 93-111.

Zak, D. E., Gonye, G. E., Schwaber, J. S., and Doyle, F. J. (2003). Importance of input perturbations and stochastic gene expression in the reverse engineering of genetic regulatory networks: insights from an identifiability analysis of an in silico network. *Gen Res* **13**: 2396-2405.